HHS Public Access

Author manuscript

Nat Genet. Author manuscript; available in PMC 2015 November 01.

Published in final edited form as:

Nat Genet. 2015 May ; 47(5): 496–504. doi:10.1038/ng.3250.

Muscle connective tissue controls development of the diaphragm and is a source of congenital diaphragmatic hernias

Allyson J. Merrell[1], **Benjamin J. Ellis**[2,3], **Zachary D. Fox**[1,3], **Jennifer A. Lawson**[1], **Jeffrey A. Weiss**[2], and **Gabrielle Kardon**[1,4]

[1]Department of Human Genetics, University of Utah, 15 North 2030 East, Salt Lake City, UT 84112

[2]Department of Bioengineering and Scientific Computing and Imaging Institute, University of Utah, 50 S Central Campus Drive, Salt Lake City, UT 84112

Abstract

The diaphragm is an essential mammalian skeletal muscle, and defects in diaphragm development are the cause of congenital diaphragmatic hernias (CDH), a common and often lethal birth defect. The diaphragm is derived from multiple embryonic sources, but how these give rise to the diaphragm is unknown and, despite the identification of many CDH-associated genes, the etiology of CDH is incompletely understood. Using mouse genetics, we show that the pleuroperitoneal folds (PPFs), transient embryonic structures, are the source of the diaphragm's muscle connective tissue, regulate muscle development, and their striking migration controls diaphragm morphogenesis. Furthermore, *Gata4* mosaic mutations in PPF-derived muscle connective tissue fibroblasts result in the development of localized amuscular regions that are biomechanically weaker and more compliant and lead to CDH. Thus the PPFs and muscle connective tissue are critical for diaphragm development and mutations in PPF-derived fibroblasts are a source of CDH.

INTRODUCTION

The muscularized diaphragm is not only a unique and defining character of all mammals[1], but is an essential skeletal muscle. Diaphragm contraction drives inspiration and is critical for respiration[2]. In addition, the diaphragm has a significant passive functional role, since it serves as a barrier between the thoracic and abdominal cavities[1]. These important functions are carried out by the costal diaphragm: a radial array of myofibers, surrounded by muscle connective tissue, that extend from the ribs to the central tendon (Fig. 1y). Development of a functional diaphragm therefore requires the coordinated morphogenesis of muscle, muscle connective tissue, and tendon, and these tissues have been suggested to develop from

[4]Corresponding author. gkardon@genetics.utah.edu.
[3]These authors contributed equally to this work.

AUTHOR CONTRIBUTIONS

A. J. M. conducted experiments, analyzed data, and wrote the manuscript. Z. J. F. conducted 2 photon experiments. B. J. E. and J. A. W. contributed FEM analysis. J. A. L. managed mouse colony. G.K. conducted experiments, analyzed data, and wrote the manuscript.

The authors declare no competing financial interests.

multiple embryonic sources[3]. However, our knowledge of how this muscle develops has been limited by the inaccessibility of mammalian embryos to classic experimental embryological techniques and lack of genetic reagents to manipulate key embryonic sources.

Defects in diaphragm development are the cause of congenital diaphragmatic hernias (CDHs), common (1/3,000 of total births) and costly (exceeding $250 million/year in the USA) birth defects[4,5]. In CDH, weaknesses in the developing diaphragm allow abdominal contents to herniate into the thoracic cavity and impede lung development. The associated lung hypoplasia is the cause of the 50% neonatal mortality and long-term morbidity associated with CDH[6]. Despite the prevalence and severity of CDH, the genetic and cellular etiology of this birth defect is incompletely understood. The majority of CDH cases appear as isolated defects[6], and the low incidence of sibling/familial recurrence suggests that CDH generally arises from *de novo* genetic mutations[7]. Molecular cytogenetic analyses of CDH patients have identified copy number variants (CNVs) in multiple chromosomal regions strongly associated with CDH[6,8,9], and detailed analyses of these regions and a limited number of mouse studies have identified over 50 candidate CDH-causative genes[8,10]. A region that contains recurrent CDH-associated CNVs is 8p23.1 (OMIM 22240)[8], and within this region variants in the *GATA binding protein 4* (*Gata4*) transcription factor have recently been shown to strongly correlate with CDH[11–13]. Nevertheless, how these candidate CDH genes mechanistically cause CDH is not clear. Functional analyses of mouse mutants have been severely limited by early embryonic lethality[14,15], low or variable incidence of CDH[16–18], and lack of conditional mutants[19,20]. Furthermore, the notable incomplete penetrance and variable expressivity of CDH-associated CNVs and genetic mutations[6,11–13] suggest that the genetic architecture underlying CDH is complex.

RESULTS

Pleuroperitoneal folds regulate diaphragm development

The diaphragm has been proposed to develop primarily from two embryonic sources. The somites are well documented to be the source of the diaphragm's muscle[21–23]. Less understood, the pleuroperitoneal folds (PPFs) are two pyramidal-shaped mesodermal structures located between the thoracic (pleural) and abdominal (peritoneal) cavities and hypothesized to be critical for diaphragm development[22]. However, without genetic reagents to label and manipulate the PPFs, it has been unclear what function they play in diaphragm development. A third embryonic structure, the septum transversum, has been suggested to be a source of the central tendon[22,24].

To test the contribution of the PPFs to diaphragm development and structure, we identified the first genetic reagent to label the PPFs. Based on the suggestion that the PPFs are of lateral plate origin[25], we tested *Prx1Cre*[26], a transgene composed of a *Prx1*-regulatory element that drives Cre-mediated recombination in the flank and limb lateral plate mesoderm (including the limb muscle connective tissue, tendons and bones). We found that when crossed with the Cre-responsive reporter *Rosa*^{LacZ}[27] it robustly labels the PPFs, but not the septum transversum (Fig. 1a, k–m, s, and data not shown). The PPFs are present at embryonic day (E) 11.5 and expand across the surface of the liver to give rise to cells throughout the diaphragm at E14.5 (Fig. 1a–d). Although *Prx1Cre* labels body wall non-

muscle tissues (Fig. 1a–e), these cells do not appear to contribute to the diaphragm (based on two-photon studies, see below). PPF cells are distinct from somite-derived muscle progenitors, myoblasts, and myofibers (Fig. 1e, k). Instead, the PPFs give rise to two non-myogenic tissues. First, in contrast to the previous hypothesis that the central tendon derives from the septum transversum[22,24], the PPFs give rise to the central tendon (Fig. 1e). Second, the PPFs give rise to muscle connective tissue fibroblasts. *Prx1*-derived cells express the muscle connective tissue marker Tcf4 (Tcf7l2)[28,29] in the E12.5 PPF (Fig. 1l) and in the fully developed diaphragm (Fig. 1x) and ultimately reside interstitial to costal (but not crural) myofibers (Fig. 1e). Importantly, the PPF cells also strongly express the CDH-implicated gene Gata4; at E12.5 most *Prx1*-derived cells express Gata4 (Fig. 1m), and all Tcf4+ fibroblasts are Gata4+ (Fig. 1q–s). Thus, we demonstrate that the PPFs are not simply transient developmental structures, but ultimately give rise to the central tendon and the muscle connective tissue fibroblasts (Fig. 1y). Furthermore, the expression in PPF cells of CDH-implicated Gata4 (as also noted in[12,16,30]) suggests that the PPFs may be important in the etiology of CDH.

To trace the contribution of myogenic cells to diaphragm morphogenesis and compare their spatiotemporal relationship to PPF cells, we genetically labeled myogenic cells using $Pax3^{Cre/+};Rosa^{LacZ/+}$ mice[31], in which Cre-mediated recombination in the somite labels all myogenic cells. Myogenic cells migrate from the somite and enter the PPFs by E11.5 (Fig. 1f, n), then spread ventrally and dorsally (Fig. 1g–i), differentiate into myofibers (Fig. 1h–i), and form a completely muscularized diaphragm by E16.5 (Fig. 1j). Comparison of muscle and PPF morphogenesis reveals that the PPFs expand ventrally in advance of the muscle (Fig. 1d, i). Labeled myogenic cells do not express either Tcf4 or Gata4, but instead are surrounded by non-myogenic Tcf4+Gata4+ cells (Fig. 1o–p). The myogenic cells' migration into the PPFs and their subsequent expansion within, but behind the leading edge of the PPF cells suggest that the PPFs may guide the morphogenesis of the diaphragmatic muscle (Fig. 1y).

If PPFs are critical for morphogenesis of the diaphragm's muscle, we expected that formation and morphogenesis of the PPFs should occur independently of muscle. To test this, we analyzed $Prx1Cre^{Tg/+};Rosa^{LacZ/+};Pax3^{SpD/SpD}$ mice[32], which have a muscleless diaphragm. We found that indeed, even in the absence of muscle, PPF cells are present and express Tcf4 and Gata4 (Fig. 1t–v) at E12.5 and subsequently undergo normal morphogenetic expansion (Fig. 1w).

The expansion of PPF cells, even in the absence of muscle, suggests that the morphogenetic movement of the PPF cells drives normal diaphragm morphogenesis. While the static images of PPF cells suggest that these cells migrate across the surface of the liver, it is formally possible that this simply reflects the dynamic activation of *Prx1Cre* and not cell movement. To test this, we cultured *ex-vivo* E12.5 diaphragms (leaving ribs and underlying liver intact) and imaged genetically labeled PPF cells via 2-photon microscopy. We found that PPF cells actively migrate across the liver surface (at the rate of 5 μm/hour); although a few cells migrate singly, most appear to migrate collectively (Fig. 1b, Supplementary Fig. 1 and Videos 1–2). This collective PPF cell migration, which occurs independent of muscle, likely drives diaphragm morphogenesis.

CDH originates with defects in PPF-derived fibroblasts

Human genetic studies have shown non-coding variants and missense mutations of *Gata4* are correlated with CDH[11–13], but explicit tests of the function of *Gata4* in development of CDH have been limited by the early embryonic lethality of *Gata4* null mice[14,15] and the reported low penetrance of CDH in *Gata4* heterozygous mice[16]. The strong Gata4 expression in the PPFs (Fig. 1 and[12,16,30]), suggests that Gata4 functions in this tissue. To test this, we generated $Prx1Cre^{Tg/+};Gata4^{\Delta/fl}$ mice (using $Gata4^{fl}$ mice[33]), in which *Gata4* is specifically deleted in the PPFs. Strikingly, we found that 100% of mutant mice (n > 33/33) develop multiple hernias throughout the diaphragm (Fig. 2a, b). Similar to CDH patients[6,34], in $Prx1Cre^{Tg/+};Gata4^{\Delta/fl}$ mice the size and location of hernias varies: most (68%) form in the dorsal lateral diaphragm (Bochdalek hernias) and the rest (32%) develop in the ventral diaphragm (Morgagni hernias, Fig. 2b). We found that hernias only occur in muscle-associated regions and not in the central tendon. Thus although the PPFs give rise to both the muscle connective tissue and the central tendon, hernias never arise in the central tendon and so it is defects in the PPF-derived muscle connective tissue that cause CDH in these mice. Unlike previous reports[16], we never observed diaphragm defects in heterozygous $Gata4^{\Delta/+}$ mice (n > 66/66, Fig. 2a). In addition, we tested whether *Gata4* was required in myogenic cells for diaphragm development by analyzing $Pax3^{Cre/+};Gata4^{\Delta/fl}$ mice. As predicted based on the lack of Gata4 expression in myogenic cells, diaphragms develop normally in these mice (n = 28/28, Fig. 2c). Because Pax3 is also expressed in neural crest cells, this rules out neural crest as a source of CDH from Gata4 mutations. Thus we definitively demonstrate that *Gata4* null mutations cause CDH. Moreover, defects in the PPFs and muscle connective tissue are a source of CDH.

Localized weaker amuscular regions give rise to hernias

Our results demonstrate that, with complete penetrance, loss of *Gata4* in PPF-derived muscle connective tissue fibroblasts results in diaphragmatic hernias, but what mechanistically causes herniation? The most commonly proposed mechanism is that hernias are caused by a morphogenetic defect in the PPFs; this defect results in a localized loss of PPF-derived tissue, a consequent absence of muscle normally associated with this tissue, formation of a hole in the diaphragm, and herniation of growing abdominal tissue through this hole[24,35]. If this hypothesis is true, PPF-derived cells, and associated muscle, should not be present in herniated regions. To test this, we examined $Prx1Cre^{Tg/+};Gata4^{\Delta/fl};Rosa^{LacZ/+}$ mice, in which PPF-derived *Gata4* null fibroblasts are β-galactosidase+ (β-gal+) and muscle is β-gal-. Surprisingly, β-gal+ fibroblasts are present as a sac covering the herniated regions, and thus these regions are not simply holes in this tissue (n = 7/7; Fig. 2g–h). Yet, the sacs are devoid of muscle, and muscle surrounding the sacs is aberrantly patterned (Fig. 2g–h). Therefore, although muscle is absent in herniated regions, hernias in $Prx1Cre^{Tg/+};Gata4^{\Delta/fl}$ mice are not caused by a failure of the morphogenetic expansion of the PPFs and the formation of holes in the diaphragm.

A second hypothesis for how CDH develops is that PPF-derived muscle connective tissue alone, without muscle, is weak and allows herniation through the weaker tissue. We tested this by examining $Prx1Cre^{Tg/+};Rosa^{LacZ/+};Pax3^{SpD/SpD}$ diaphragms, in which muscle is absent but PPF-derived muscle connective tissue is present (Fig. 1w). However, in these

mice with muscleless diaphragms, hernias never formed (n > 10/10, Fig. 2d, i). This demonstrates that PPF-derived muscle connective tissue alone, even in the absence of muscle, is sufficiently strong to prevent herniation of abdominal tissues.

These data suggest two additional hypotheses for the mechanism underlying herniation. First, the muscle connective tissue produced by *Gata4* null fibroblasts may be weaker than connective tissue made by wild-type fibroblasts and this weaker tissue allows for herniation of abdominal tissue. Alternatively, formation of relatively weak regions of amuscular connective tissue juxtaposed to stronger muscularized regions may allow abdominal contents to herniate through the localized weak regions. To test this, we generated $Prx1Cre^{Tg/+};Gata4^{\Delta/fl};Pax3^{SpD/SpD}$ mice, in which diaphragms are muscleless and the PPF-derived fibroblasts are *Gata4* null. If the first hypothesis is correct, then hernias should form, while if the second hypothesis is correct, hernias should be absent. Strikingly, no hernias develop in these mice (n = 3/3), and the diaphragms are indistinguishable from $Pax3^{SpD/SpD}$ mice (Fig. 2d–e, i–j). Thus the loss of muscle rescues the herniation phenotype of $Prx1Cre^{Tg/+};Gata4^{\Delta/fl}$ mice. This demonstrates that the muscle connective tissue produced by *Gata4* null fibroblasts is not inherently weaker than wild-type connective tissue. Instead, hernias only develop when localized regions of amuscular connective tissue develop in juxtaposition with muscularized regions; through these amuscular regions that are relatively weaker than muscularized regions, abdominal tissue herniates.

To gain further insight into the biomechanics governing herniation, we turned to finite element modeling. The amuscular regions of E16.5 diaphragms, prior to overt herniation of abdominal tissue, are 25% of the thickness of the muscular regions (see Fig. 4c, g). This suggests that the relative weakness of the amuscular compared to the muscular regions could simply be due to its decreased thickness. Alternatively, the amuscular regions may be both thinner and composed of a more compliant material than muscle. We tested this by creating a finite element model. The geometry of the diaphragm was based on the dimensions of an E16.5 mutant diaphragm (see Fig. 4c), and a uniform physiologically reasonable pressure was applied to the diaphragm to simulate the pressure of the growing liver. Using the FEBio nonlinear finite element solver[36], when the muscle material behavior is represented by an isotropic hyperelastic constitutive equation (based on[37]) and the amuscular region is made significantly more compliant (deforms more in response to an applied force) than the muscle, a pressure of 380 Pa induced a bulge in the amuscular region that matched the geometry of the hernias in experimental mice (Model B, Fig. 2 k, m, Supplementary Videos 3–4). In contrast, when the thinner amuscular region was assigned the same material properties as the muscle, pressures up to 380 Pa were unable to generate a bulge in the amuscular region (Model A, Fig. 2k–l). Together these results indicate that the weakness in the amuscular regions is due to both its decreased thickness and increased compliance as compared with the muscularized regions.

Herniated tissue physically impedes lung development

The neonatal mortality and long-term morbidity of CDH patients is caused by secondary lung hypoplasia, which is thought to arise from the physical impedance of lung growth by the herniated abdominal tissue. However, a “dual-hit hypothesis” has also been proposed[38],

whereby lung hypoplasia can result both from physical impedance by herniated tissue and from cell-autonomous effects on lung development by CDH-associated genes. Consistent with this hypothesis, mutations in *Gata4* can cell-autonomously affect lung development[39]. Similar to CDH patients, *Prx1Cre*$^{Tg/+}$;*Gata4*$^{\Delta/fl}$ mice have low O_2 blood saturation (as measured by pulse oximetry; data not shown) and most die within a few hours of birth. Defects in the lung lobar structure were found in all mice examined (n = 8/8, Fig. 3a–b, e–f, i–j) and resulted in up to a 34% reduction in lung volume (as quantified by microCT) of lobes adjacent to hernias (Fig. 3i–k; Supplementary Videos 5–6). The tight correlation of lung defects with hernias in all mice strongly suggests that the herniated tissue physically impedes lung growth in these mice. Furthermore, the absence of lung defects in *Prx1Cre*$^{Tg/+}$;*Gata4*$^{\Delta/fl}$;*Pax3*$^{SpD/SpD}$ mice (Fig. 3c–d, g–h) argues that herniation precedes and causes lung hypoplasia. Thus *Prx1Cre*$^{Tg/+}$;*Gata4*$^{\Delta/fl}$ mice not only develop CDH, but also the lung defects and neonatal lethality typically accompanying CDH, and impedance of lung growth by herniated tissue is sufficient to induce lung lobar defects. It is also likely that *Gata4* mutations have additional cell-autonomous effects on lung development (as shown by[39]), although we could not directly evaluate this, as *Prx1Cre* has limited recombination in the lungs and the alveolar structure is largely unaffected in these mutant mice (Supplementary Fig. 2a–c).

Aberrant HGF and muscle proliferation and apoptosis in CDH

Our experiments demonstrate that hernias form when localized amuscular regions develop within the muscular diaphragm. To determine when hernias and amuscular regions arise, we examined a developmental time series of mutant *Prx1Cre*$^{Tg/+}$;*Gata4*$^{\Delta/fl}$ embryos. Overt herniation of liver through the diaphragm first occurs at E16.5 (Fig. 4a, e). However, defects in muscle are present by E14.5 (Fig. 4b, f), and neither differentiated myofibers nor muscle progenitors are present in amuscular regions (Fig. 4c–d, g–h). Even at E12.5 there is a profound defect in the number and localization of muscle progenitors (Fig. 4i–j).

A critical early regulator of muscle progenitors migrating into the limb and diaphragm is Hepatocyte Growth Factor (HGF)[23,40,41] and therefore an attractive candidate downstream target of Gata4. We found in control mice that the PPF cells, independent of the presence of muscle, robustly express the ligand *HGF* E12-13.5 (Fig. 5a–c), while the muscle progenitors express the HGF receptor, Met (data not shown). In *Prx1Cre*$^{Tg/+}$;*Gata4*$^{\Delta/fl}$ E12.5 diaphragms, *HGF* is markedly down-regulated and diminished in regions that consistently give rise to hernias (n = 11/11, Fig. 5d).

HGF functions as a mitogen and a cell survival factor[42], and therefore we examined whether changes in apoptosis and proliferation determine why fewer muscle progenitors are present in mutant embryos. At E12.5 in the developing diaphragm of control embryos, few TUNEL + apoptotic cells are present (Fig. 6a, c–e, Supplementary Video 7), while nearly all muscle progenitors are actively proliferating (Fig. 6i, k–m, Supplementary Video 9). In contrast, in mutant embryos there is a marked increase in apoptotic cells, many of which are present in regions that are abnormally devoid of muscle and consistently give rise to hernias (Fig. 6b, f–h, Supplementary Video 8). In addition, there is a profound decrease in EdU+ proliferative cells (Fig. 6j, n–p, Supplementary Video 10). Similar to the heart[43,44], we find that loss of

Gata4 leads to decreased levels of cell cycle regulators Cyclin D2 and Cdk4 in PPF cells (Supplementary Fig. 3a–l). In culture, isolated *Gata4* null PPF fibroblasts proliferate at less than half the level of wild-type fibroblasts (Supplementary Fig. 4a). Moreover, when diaphragm myogenic cells are cultured with PPF cells, *Gata4* null fibroblasts (as compared with wild-type fibroblasts) fail to support the growth of myogenic cells (Supplementary Fig. 4b–c).

In mutant diaphragms, the number of muscle progenitors is greatly reduced by increased cell death and decreased proliferation, but how do localized amuscular regions develop? In control $Prx1Cre^{Tg/+};Gata^{fl/+};Rosa^{mTmG/+}$ embryos, muscle progenitors migrate into and develop completely surrounded by GFP+ PPF cells (Fig. 6a, i; Supplementary Videos 7, 9). As the PPF cells expand they carry with them the proliferating and differentiating myogenic cells. In contrast, in $Prx1Cre^{Tg/+};Gata4^{\Delta/fl};Rosa^{mTmG/+}$ mutants, at E12.5 myogenic cells are largely excluded from GFP+Gata4− regions (Fig. 6b, j; Supplementary Videos 8,10). These localized amuscular regions likely result from the mosaic deletion of one *Gata4* allele by the *Prx1Cre* transgene which does not efficiently recombine in all PPF cells at E11.5–12.5 (Supplementary Fig. 2d–i; the other *Gata4* allele is deleted in the germline); muscle is excluded from the PPF regions where *Gata4* has been deleted during this early time window. Only during this early time are myogenic cells sensitive to *Gata4*, as deletion of *Gata4* via $Tcf4^{Cre29}$, which causes recombination in PPF fibroblasts primarily after E12.5, does not result in hernias (n = 16/16, data not shown). Altogether these data indicate that early mosaic deletion of *Gata4* in PPF cells leads to increased apoptosis and decreased proliferation of muscle progenitors and the development of localized amuscular regions, which ultimately allow herniation (Fig. 7).

DISCUSSION

Our study establishes that the PPFs and muscle connective tissue fibroblasts, although previously underappreciated, are critical for the development of the diaphragm and CDH. PPF cells not only give rise to the diaphragm's muscle connective tissue and the central tendon, but the connective tissue fibroblasts control the morphogenesis of the diaphragm's muscle. Our finding that the connective tissue regulates muscle development has precedence, as muscle connective tissue fibroblasts regulate the pattern of limb muscles[28] and the fiber-type of limb and diaphragm muscles[29]. Completely novel is our finding that the active, apparently collective, cell migration of connective tissue fibroblasts across the liver's surface controls the expansion of muscle progenitors and overall diaphragm morphogenesis.

We also definitively demonstrate for the first time that defects in the muscle connective tissue fibroblast component of the PPFs are a cellular source of CDH and *Gata4* null mutations in these cells cause CDH. Surprisingly, we show that hernias do not result from defects in PPF cell migration and the formation of holes in the diaphragm. Instead, PPF deletion of *Gata4* leads to the development of localized amuscular regions through which the growing liver and intestines herniate. In humans, such hernias with connective tissue surrounding the herniated tissue are classified as "sac hernias"[6], and we hypothesize that many hernias are covered by connective tissue early in development. Mechanistically, CDH

arises when thinner and more compliant amuscular regions develop within the thicker and stiffer muscularized diaphragm and allow herniation. Development of the amuscular regions in mutants results from a marked decrease in cell proliferation, an increase in cell death and, most notably, the localized exclusion of myogenic cells from regions with early PPF deletion of *Gata4* and down-regulation of HGF expressed by the muscle connective tissue fibroblasts. Thus we elucidate how defects in the muscle connective tissue are a potent source of CDH. CDH has been associated with over 50 candidate genes and recently several alternative mechanisms of CDH have been described[45,46]. An important area of future research will be to determine whether CDH is of heterogeneous origin or if any cellular or molecular defect is common to the etiology of CDH.

Our data suggests a novel genetic hypothesis for the origin of CDH. Our finding that CDH derives from localized, weaker amuscular regions that develop specifically where *Gata4* has been mutated early in muscle connective tissue fibroblasts suggests that somatic mosaic mutations in fibroblasts may be a genetic feature of some CDH patients. A potential role for somatic mosaicism in CDH has previously been suggested by the largely discordant occurrence of CDH in monozygotic twins[47], including twins with an 8p23.1 deletion[48], and the finding of genetic mosaicism in CDH patients[49,50]. Our hypothesis that CDH can arise from somatic mosaic mutations may explain the notable incomplete penetrance and variable expressivity of many CDH-associated CNVs and genetic mutations, particularly *Gata4*[11–13,48]. Interestingly, in humans *Gata4* haploinsufficiency and in mice 70% reduction in *Gata4* expression leads with nearly complete penetrance to heart defects[12,48,51]. In contrast, in humans *Gata4* haploinsufficiency is incompletely penetrant for CDH[12,48], and in mice *Gata4* heterozygotes either do not develop CDH (our data) or do so with low penetrance[16,52]. In addition, for CDH patients with shared *Gata4* missense mutations[13] or intronic variants[11], the location and severity of hernias is highly variable. Our data suggest the hypothesis that loss of one *Gata4* allele confers susceptibility, but is not sufficient to cause CDH; development of CDH requires somatic loss of a second allele in a subset of the connective tissue fibroblasts early during diaphragm morphogenesis. When and where this second allele is deleted determines the size and location of the amuscular region and hernia (i.e. CDH expressivity). In humans, somatic mosaicism in *Gata4* mutations and 8p23.1 polymorphisms are well documented[53–56]. Alternatively, the second somatic mosaic, CDH-causative mutation may not be loss of the second *Gata4* allele, but another CDH-associated gene (resulting in non-allelic non-complementation); multiple CDH-associated genes are strongly expressed in the PPF cells, including *Zfpm2*[19] and *Nr2f2*[18] which are known to genetically interact with *Gata4*. Thus the genetic architecture underlying CDH may be complex.

In summary, although muscle connective tissue has often been relegated to a role supporting muscle structure and function, we demonstrate that muscle connective tissue fibroblasts dynamically control diaphragm morphogenesis and their interactions with muscle progenitors critically regulate the development of the diaphragm's muscle and are a source of CDH. The role of mosaicism in human disease has received increasing attention in recent years[57]. Here we show in mice that mosaic mutations in muscle connective tissue have profound cellular and biomechanical consequences and lead to hernias. We hypothesize that

early somatic mosaic mutations are critical for the etiology of CDH in humans, and this hypothesis will be tested in future experiments.

Online Methods

Materials and Methods

Mice—All mice have been previously published. We used *Prx1*^{Cre}[26], *Pax3*^{Cre}[31], and *HPRT*^{Cre}[58] Cre alleles; *Rosa*^{LacZ}[27] and *Rosa*^{mTmG}[59] Cre-responsive reporter alleles; and *Pax3*^{SpD}[32], *Gata4*^{fl}[33] mutant alleles. *Gata4*$^{del/+}$ mice were generated by breeding *Gata4*^{fl} mice to *HPRT*^{Cre} mice. Mice were back-crossed on to C57/Bl6J background. No statistical method was used to predetermine sample size; all animals were included; and the experiments were not randomized. Animal experiments were performed in accordance with protocols approved by the Institutional Animal Care and Use Committee at the University of Utah.

Immunofluorescence, β-Galactosidase staining, and microscopy—For section immunofluorescence, embryos were fixed, embedded, cryosectioned, and immunostained as described previously[29]. EdU (Life Technologies) was detected per manufacturer's directions. For whole mount immunofluorescence, embryos were fixed 24 h in 4% PFA, dissected, incubated 24 hours in Dent's bleach (1:2 30% H_2O_2:Dent's fix), and stored in Dent's fix (1:4 DMSO:MeOH) for at least 5 days. Embryos were washed in PBS, blocked 1h in 5% serum + 20% DMSO, incubated in primary antibody at room temperature 48 h, washed in PBS, incubated in secondary antibody 48 h, washed in PBS, and subjected to EdU reaction 1 h. Diaphragms were cleared in BABB (33% Benzyl Alcohol, 66% Benzyl Benzoate). AP-conjugated mouse IgG1 α My32 was incubated for 48 h and detected with 250 μg/ml NBT and 125 μg/ml BCIP (Sigma) in NTMT.

Cultured cells were fixed for 20 minutes in 4% PFA, blocked in 5% serum in PBS with 0.1% Triton X-100 for 1 h, incubated in primary antibody at 4°C overnight, washed with PBS, and incubated for two hours in secondary antibody. Following antibody staining, EdU was detected as above. Cells were incubated in 0.4 ug/ml Hoechst for 5 minutes and mounted with Fluoromount-G.

Antibodies are listed in Supplementary Table 1.

For whole-mount β-galactosidase staining, embryos were fixed 1.5 hours in 4% PFA + 2mM $MgCl_2$. Diaphragms were dissected, washed in PBS and rinse buffer (100mM Sodium Phosphate, 2mM $MgCl_2$, 0.01% Na Deoxycholate, 0.02% Ipegal) and stained 16 h at 37°C in X-gal staining solution (5mM potassium ferricyanide, 5 mM potassium ferrocyanide, 1 mg/ml Xgal).

Fluorescent images were taken on a Nikon A1 confocal. Optical stacks of whole-mounts were rendered using FluoRender[60]. β-galactosidase stained embryos were imaged with a Qimaging camera. All analyses were performed blinded.

Cell Culture—Fibroblasts were isolated from E15.5 *Gata4$^{fl/fl}$;Rosa$^{mTmG/+}$* or *Rosa$^{mTmG/+}$* diaphragms, cultured, and expanded 3 weeks. 4 μM TAT-Cre (M Hockin, MR Capecchi) was added to induce recombination. EdU was given 4 h prior to fixation and immunofluorescence. For co-cultures, fibroblasts and myoblasts were isolated from E15.5 *Prx1Cre$^{Tg/+}$;Gata4$^{del/fl}$;Rosa$^{mTmG/+}$* or *Prx1Cre$^{+/+}$;Gata4$^{del/fl}$;Rosa$^{mTmG/+}$* diaphragms, cultured 2 days, and given EdU 1 h prior to fixation and immunofluorescence. Statistical significance was performed with 2-tailed Student's t test.

Diaphragm Explants—E12.5 *Prx1Cre$^{Tg/+}$;Rosa$^{mTmG/+}$* mice were harvested and trimmed to only include the diaphragm with attached ribs, hind limbs, and liver. Explanted diaphragms were cultured 2–6 h in 100% horse serum, at 37°C, in the presence of 5% CO_2. Explants were imaged on a Bruker (Prairie) 2 Photon microscope, and 4-dimensional datasets were rendered and visualized using FluoRender[60]. Individual cells were tracked using FluoRender.

Modeling—To gain insights into the biomechanics of herniation, we used finite element modeling, a computational method for assembling the response of a complex system from individual contributions of discrete elements[36]. The finite element model of hernia development was based on an E16.5 *Prx1Cre$^{Tg/+}$;Gata4$^{\Delta/fl}$* herniated mouse diaphragm. The geometry of the diaphragm was based on surfaces created from segmenting microscopy images. Surfaces were discretized with quadratic-tetrahedral elements, and adequacy of the spatial discretization was confirmed with a mesh convergence study. Meshes were created with ANSA software (BETA CAE Systems USA) and analyzed with FEBio[36]. For the simulations, the rib cage surrounding the diaphragm was rigidly constrained in the model (kept immobile), while a uniform pressure of 380 Pa was applied to simulate the pressure applied by the liver. The pressure was chosen so that the bulge height of the muscle region predicted by the model matched the height measured in the experiment. The muscle was represented with an isotropic hyperelastic Veronda-Westmann constitutive equation[61] with coefficients (C_1 = 2.1 MPa, C_2 = 0.1, K = 10) based on published data[37]. The connective tissue of the hernia was represented with an isotropic hyperelastic Mooney-Rivlin constitutive equation[62] using either the coefficients C_1 = 0.003 MPa, K = 1 or C_1 = 0.01 MPa, K = 10.

MicroCT Analysis of Lungs—Embryos were fixed in 4% PFA in PBS overnight. Lungs were removed, pre-treated with 25% Lugol's solution for 1 hour, and then soaked in PBS for 1 hour prior to imaging. CT images consisting of 360 degrees and 600 projections were acquired by using an Inveon trimodality PET/SPECT/CT scanner (Siemens Preclinical Solutions, Knoxville, TN). The exposure time was 2.9 seconds with detector settings at 80 kVp and 150 μA. Data was reconstructed onto a 1792×1792×2688 image matrix using the COBRA software package (Exxim Computing Corporation, Pleasanton, CA). The effective image voxel size was 33.6 μm isotropic. Reconstructed images were analyzed using Osirix software.

Supplementary Material

Refer to Web version on PubMed Central for supplementary material.

ACKNOWLEDGEMENTS

We thank C. Rodesch at the U of Utah Imaging Core for help with microscopy, Samer Merchant for help with microCT imaging, Y. Wan and C. Hansen for Fluorender analysis, M Hockin and MR Capecchi for Cre protein, and M Colasanto, N Elde, LB Jorde, A Keefe, A Letsou, LC Murtaugh, CJ Tabin for critical comments on the manuscript. AJM was supported by U of Utah Graduate Fellowship, FEBio is supported by NIH R01GMo83925 to JA Weiss and GA Ateshian and Fluorender is supported by NIH R01-GM098151 to C Hansen. This research was supported by NIH R01 HD053728 and March of Dimes FY12-405 to GK.

REFERENCES

1. Perry SF, Similowski T, Klein W, Codd JR. The evolutionary origin of the mammalian diaphragm. Respir Physiol Neurobiol. 2010; 171:1–16. [PubMed: 20080210]
2. Campbell, EJM.; Agostoni, E.; Newsom Davis, J. The Respiratory Muscles: Mechanics and Neural Control. London: Lloyd-Luke; 1970.
3. Merrell AJ, Kardon G. Development of the diaphragm -- a skeletal muscle essential for mammalian respiration. FEBS J. 2013; 280:4026–4035. [PubMed: 23586979]
4. Raval MV, Wang X, Reynolds M, Fischer AC. Costs of congenital diaphragmatic hernia repair in the United States-extracorporeal membrane oxygenation foots the bill. J Pediatr Surg. 2011; 46:617–624. [PubMed: 21496527]
5. Torfs CP, Curry CJ, Bateson TF, Honore LH. A population-based study of congenital diaphragmatic hernia. Teratology. 1992; 46:555–565. [PubMed: 1290156]
6. Pober BR. Overview of epidemiology, genetics, birth defects, and chromosome abnormalities associated with CDH. Am J Med Genet C Semin Med Genet. 2007; 145C:158–171. [PubMed: 17436298]
7. Pober BR, et al. Infants with Bochdalek diaphragmatic hernia: sibling precurrence and monozygotic twin discordance in a hospital-based malformation surveillance program. Am J Med Genet A. 2005; 138A:81–88. [PubMed: 16094667]
8. Holder AM, et al. Genetic factors in congenital diaphragmatic hernia. Am J Hum Genet. 2007; 80:825–845. [PubMed: 17436238]
9. Veenma DC, de Klein A, Tibboel D. Developmental and genetic aspects of congenital diaphragmatic hernia. Pediatr Pulmonol. 2012; 47:534–545. [PubMed: 22467525]
10. Russell MK, et al. Congenital diaphragmatic hernia candidate genes derived from embryonic transcriptomes. Proc Natl Acad Sci U S A. 2012; 109:2978–2983. [PubMed: 22315423]
11. Arrington CB, et al. A family-based paradigm to identify candidate chromosomal regions for isolated congenital diaphragmatic hernia. Am J Med Genet A. 2012; 158A:3137–3147. [PubMed: 23165927]
12. Longoni M, et al. Congenital diaphragmatic hernia interval on chromosome 8p23.1 characterized by genetics and protein interaction networks. Am J Med Genet A. 2012; 158A:3148–3158. [PubMed: 23165946]
13. Yu L, et al. Variants in GATA4 are a rare cause of familial and sporadic congenital diaphragmatic hernia. Hum Genet. 2013; 132:285–292. [PubMed: 23138528]
14. Kuo CT, et al. GATA4 transcription factor is required for ventral morphogenesis and heart tube formation. Genes Dev. 1997; 11:1048–1060. [PubMed: 9136932]
15. Molkentin JD, Lin Q, Duncan SA, Olson EN. Requirement of the transcription factor GATA4 for heart tube formation and ventral morphogenesis. Genes Dev. 1997; 11:1061–1072. [PubMed: 9136933]
16. Jay PY, et al. Impaired mesenchymal cell function in Gata4 mutant mice leads to diaphragmatic hernias and primary lung defects. Dev Biol. 2007; 301:602–614. [PubMed: 17069789]
17. Mendelsohn C, et al. Function of the retinoic acid receptors (RARs) during development (II). Multiple abnormalities at various stages of organogenesis in RAR double mutants. Development. 1994; 120:2749–2771. [PubMed: 7607068]
18. You LR, et al. Mouse lacking COUP-TFII as an animal model of Bochdalek-type congenital diaphragmatic hernia. Proc Natl Acad Sci U S A. 2005; 102:16351–16356. [PubMed: 16251273]

19. Ackerman KG, et al. Fog2 is required for normal diaphragm and lung development in mice and humans. PLoS Genet. 2005; 1:58–65. [PubMed: 16103912]
20. Coles GL, Ackerman KG. Kif7 is required for the patterning and differentiation of the diaphragm in a model of syndromic congenital diaphragmatic hernia. Proc Natl Acad Sci U S A. 2013; 110:E1898–E1905. [PubMed: 23650387]
21. Allan DW, Greer JJ. Embryogenesis of the phrenic nerve and diaphragm in the fetal rat. J Comp Neurol. 1997; 382:459–468. [PubMed: 9184993]
22. Babiuk RP, Zhang W, Clugston R, Allan DW, Greer JJ. Embryological origins and development of the rat diaphragm. J Comp Neurol. 2003; 455:477–487. [PubMed: 12508321]
23. Dietrich S, et al. The role of SF/HGF and c-Met in the development of skeletal muscle. Development. 1999; 126:1621–1629. [PubMed: 10079225]
24. Greer JJ, et al. Structure of the primordial diaphragm and defects associated with nitrofen-induced CDH. J Appl Physiol. 2000; 89:2123–2129. [PubMed: 11090558]
25. Ackerman KG, Greer JJ. Development of the diaphragm and genetic mouse models of diaphragmatic defects. Am J Med Genet C Semin Med Genet. 2007; 145C:109–116. [PubMed: 17436296]
26. Logan M, et al. Expression of Cre Recombinase in the developing mouse limb bud driven by a Prxl enhancer. Genesis. 2002; 33:77–80. [PubMed: 12112875]
27. Soriano P. Generalized lacZ expression with the ROSA26 Cre reporter strain. Nat Genet. 1999; 21:70–71. [PubMed: 9916792]
28. Kardon G, Harfe BD, Tabin CJ. A Tcf4-positive mesodermal population provides a prepattern for vertebrate limb muscle patterning. Dev Cell. 2003; 5:937–944. [PubMed: 14667415]
29. Mathew SJ, et al. Connective tissue fibroblasts and Tcf4 regulate myogenesis. Development. 2011; 138:371–384. [PubMed: 21177349]
30. Clugston RD, Zhang W, Greer JJ. Gene expression in the developing diaphragm: significance for congenital diaphragmatic hernia. Am J Physiol Lung Cell Mol Physiol. 2008; 294:L665–L675. [PubMed: 18263670]
31. Engleka KA, et al. Insertion of Cre into the Pax3 locus creates a new allele of Splotch and identifies unexpected Pax3 derivatives. Dev Biol. 2005; 280:396–406. [PubMed: 15882581]
32. Vogan KJ, Epstein DJ, Trasler DG, Gros P. The splotch-delayed (Spd) mouse mutant carries a point mutation within the paired box of the Pax-3 gene. Genomics. 1993; 17:364–369. [PubMed: 8406487]
33. Watt AJ, Battle MA, Li J, Duncan SA. GATA4 is essential for formation of the proepicardium and regulates cardiogenesis. Proc Natl Acad Sci U S A. 2004; 101:12573–12578. [PubMed: 15310850]
34. Ackerman KG, et al. Congenital diaphragmatic defects: proposal for a new classification based on observations in 234 patients. Pediatr Dev Pathol. 2012; 15:265–274. [PubMed: 22257294]
35. Clugston RD, Greer JJ. Diaphragm development and congenital diaphragmatic hernia. Semin Pediatr Surg. 2007; 16:94–100. [PubMed: 17462561]
36. Maas SA, Ellis BJ, Ateshian GA, Weiss JA. FEBio: finite elements for biomechanics. J Biomech Eng. 2012; 134:011005. [PubMed: 22482660]
37. Strumpf RK, Humphrey JD, Yin FC. Biaxial mechanical properties of passive and tetanized canine diaphragm. Am J Physiol. 1993; 265:H469–H475. [PubMed: 8368350]
38. Keijzer R, Liu J, Deimling J, Tibboel D, Post M. Dual-hit hypothesis explains pulmonary hypoplasia in the nitrofen model of congenital diaphragmatic hernia. Am J Pathol. 2000; 156:1299–1306. [PubMed: 10751355]
39. Ackerman KG, et al. Gata4 is necessary for normal pulmonary lobar development. Am J Respir Cell Mol Biol. 2007; 36:391–397. [PubMed: 17142311]
40. Bladt F, Riethmacher D, Isenmann S, Aguzzi A, Birchmeier C. Essential role for the c-met receptor in the migration of myogenic precursor cells into the limb bud. Nature. 1995; 376:768–771. [PubMed: 7651534]
41. Maina F, et al. Uncoupling of Grb2 from the Met receptor in vivo reveals complex roles in muscle development. Cell. 1996; 87:531–542. [PubMed: 8898205]

42. Nakamura K, Hongo A, Kodama J, Hiramatsu Y. The role of hepatocyte growth factor activator inhibitor (HAI)-1 and HAI-2 in endometrial cancer. Int J Cancer. 2011; 128:2613–2624. [PubMed: 20715109]
43. Rojas A, et al. GATA4 is a direct transcriptional activator of cyclin D2 and Cdk4 and is required for cardiomyocyte proliferation in anterior heart field-derived myocardium. Mol Cell Biol. 2008; 28:5420–5431. [PubMed: 18591257]
44. Yamak A, et al. Cyclin D2 rescues size and function of GATA4 haplo-insufficient hearts. Am J Physiol Heart Circ Physiol. 2012; 303:H1057–H1066. [PubMed: 22923619]
45. Domyan ET, et al. Roundabout receptors are critical for foregut separation from the body wall. Dev Cell. 2013; 24:52–63. [PubMed: 23328398]
46. Zhang B, et al. Heparan sulfate deficiency disrupts developmental angiogenesis and causes congenital diaphragmatic hernia. J Clin Invest. 2014; 124:209–221. [PubMed: 24355925]
47. Veenma D, et al. Copy number detection in discordant monozygotic twins of Congenital Diaphragmatic Hernia (CDH) and Esophageal Atresia (EA) cohorts. Eur J Hum Genet. 2012; 20:298–304. [PubMed: 22071887]
48. Wat MJ, et al. Chromosome 8p23.1 deletions as a cause of complex congenital heart defects and diaphragmatic hernia. Am J Med Genet A. 2009; 149A:1661–1677. [PubMed: 19606479]
49. Kantarci S, et al. Characterization of the chromosome 1q41q42.12 region, and the candidate gene DISP1, in patients with CDH. Am J Med Genet A. 2010; 152A:2493–2504. [PubMed: 20799323]
50. Veenma D, et al. Comparable low-level mosaicism in affected and non affected tissue of a complex CDH patient. PLoS One. 2010; 5:e15348. [PubMed: 21203572]
51. Pu WT, Ishiwata T, Juraszek AL, Ma Q, Izumo S. GATA4 is a dosage-sensitive regulator of cardiac morphogenesis. Dev Biol. 2004; 275:235–244. [PubMed: 15464586]
52. Wat MJ, et al. Mouse model reveals the role of SOX7 in the development of congenital diaphragmatic hernia associated with recurrent deletions of 8p23.1. Hum Mol Genet. 2012; 21:4115–4125. [PubMed: 22723016]
53. Bosch N, et al. Nucleotide, cytogenetic and expression impact of the human chromosome 8p23.1 inversion polymorphism. PLoS One. 2009; 4:e8269. [PubMed: 20011547]
54. Giglio S, et al. Olfactory receptor-gene clusters, genomic-inversion polymorphisms, and common chromosome rearrangements. Am J Hum Genet. 2001; 68:874–883. [PubMed: 11231899]
55. Reamon-Buettner SM, Borlak J. GATA4 zinc finger mutations as a molecular rationale for septation defects of the human heart. J Med Genet. 2005; 42:e32. [PubMed: 15863664]
56. Reamon-Buettner SM, Cho SH, Borlak J. Mutations in the 3'-untranslated region of GATA4 as molecular hotspots for congenital heart disease (CHD). BMC Med Genet. 2007; 8:38. [PubMed: 17592645]
57. Biesecker LG, Spinner NB. A genomic view of mosaicism and human disease. Nat Rev Genet. 2013; 14:307–320. [PubMed: 23594909]

METHODS REFERENCES

1. Logan M, et al. Expression of Cre Recombinase in the developing mouse limb bud driven by a Prxl enhancer. Genesis. 2002; 33:77–80. [PubMed: 12112875]
2. Engleka KA, et al. Insertion of Cre into the Pax3 locus creates a new allele of Splotch and identifies unexpected Pax3 derivatives. Dev Biol. 2005; 280:396–406. [PubMed: 15882581]
3. Tang SH, Silva FJ, Tsark WM, Mann JR. A Cre/loxP-deleter transgenic line in mouse strain 129S1/SvImJ. Genesis. 2002; 32:199–202. [PubMed: 11892008]
4. Soriano P. Generalized lacZ expression with the ROSA26 Cre reporter strain. Nat Genet. 1999; 21:70–71. [PubMed: 9916792]
5. Muzumdar MD, Tasic B, Miyamichi K, Li L, Luo L. A global double-fluorescent Cre reporter mouse. Genesis. 2007; 45:593–605. [PubMed: 17868096]
6. Vogan KJ, Epstein DJ, Trasler DG, Gros P. The splotch-delayed (Spd) mouse mutant carries a point mutation within the paired box of the Pax-3 gene. Genomics. 1993; 17:364–369. [PubMed: 8406487]

7. Watt AJ, Battle MA, Li J, Duncan SA. GATA4 is essential for formation of the proepicardium and regulates cardiogenesis. Proc Natl Acad Sci U S A. 2004; 101:12573–12578. [PubMed: 15310850]
8. Mathew SJ, et al. Connective tissue fibroblasts and Tcf4 regulate myogenesis. Development. 2011; 138:371–384. [PubMed: 21177349]
9. Wan Y, Otsuna H, Chien CB, Hansen C. An interactive visualization tool for multi-channel confocal microscopy data in neurobiology research. IEEE Trans Vis Comput Graph. 2009; 15:1489–1496. [PubMed: 19834225]
10. Maas SA, Ellis BJ, Ateshian GA, Weiss JA. FEBio: finite elements for biomechanics. J Biomech Eng. 2012; 134:011005. [PubMed: 22482660]
11. Veronda DR, Westmann RA. Mechanical characterization of skin-finite deformations. J Biomech. 1970; 3:111–124. [PubMed: 5521524]
12. Strumpf RK, Humphrey JD, Yin FC. Biaxial mechanical properties of passive and tetanized canine diaphragm. Am J Physiol. 1993; 265:H469–H475. [PubMed: 8368350]
13. Mooney M. A theory of large elastic deformation. Journal of Applied Physics. 1940; 11:582–592.

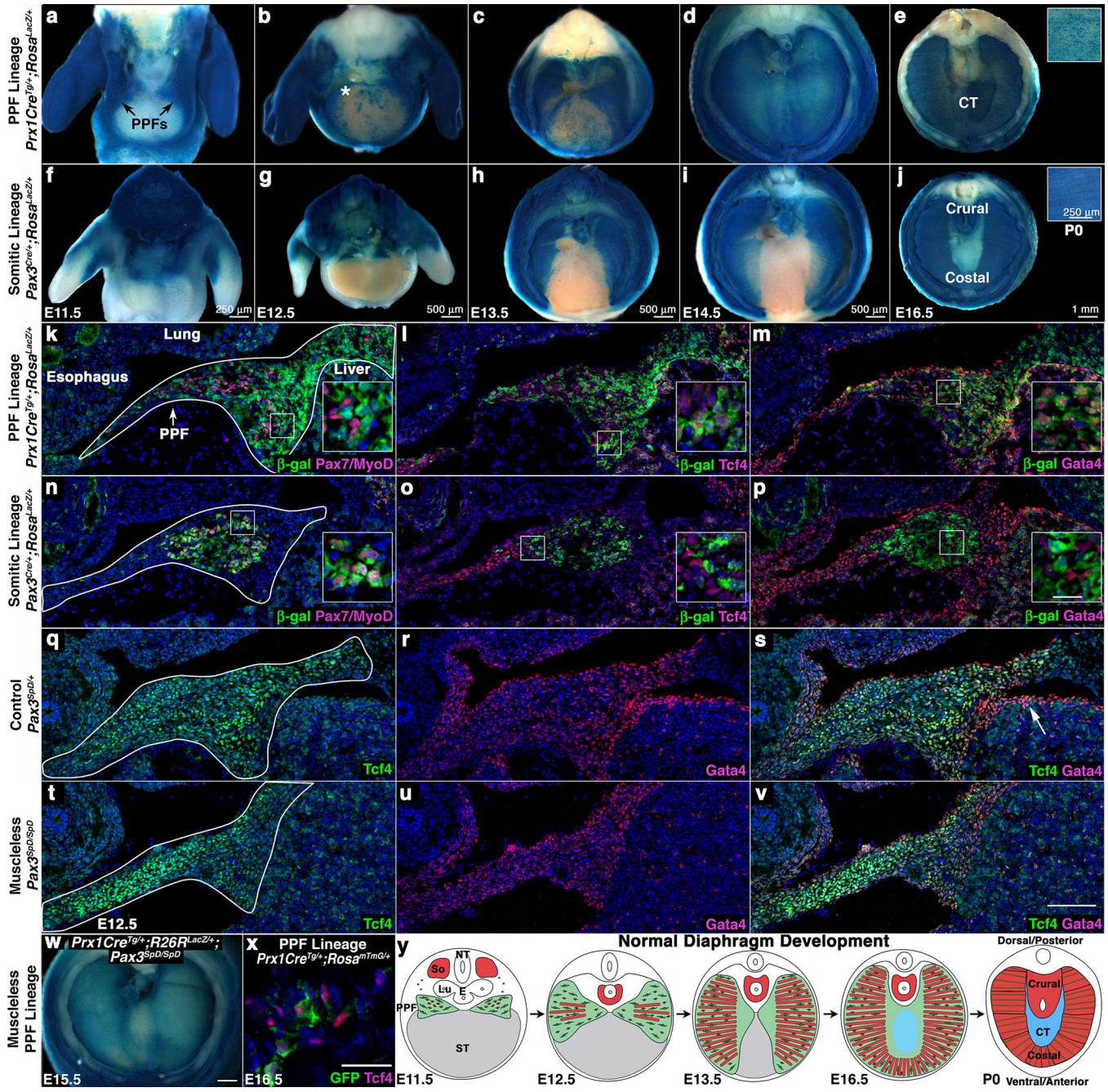

Fig. 1. PPFs contains Gata4+ muscle connective tissue fibroblasts that migrate independently and in advance of myogenic cells

(**a–e**) *Prx1Cre*^{Tg} labels PPF cells (**a**) that expand throughout diaphragm (**d**) and contribute to the central tendon (**e**) and costal muscle connective tissue fibroblasts (inset **e**) As expected, *Prx1Cre*^{Tg} labels limb and body wall lateral plate mesoderm. (**f–j**) *Pax3*^{Cre} labels myogenic cells (**f**) that give rise to crural and costal muscles (**j**). (**k–m**) *Prx1Cre*^{Tg} does not label Pax7+ muscle progenitors or MyoD+ myoblasts (**k**), but labels Tcf4+ (**l**) and Gata4+ (**m**) fibroblasts in the PPFs. (**n–p**) *Pax3*^{Cre} labels Pax7+/MyoD+ myogenic cells (**n**), but not Tcf4+ (**o**) or Gata4+ cells (**p**). n > 3/time point. (**q–v**) Gata4+ cells are Tcf4+ muscle

connective tissue fibroblasts (**q–s**) and present in the absence of muscle (**t–v**). **w–x**, *Prx1*-derived cells expand in absence of muscle (**w**, n = 4/4) and are Tcf4+ (**x**). (**y**) Model of diaphragm development. (**a–j**). n > 5 for each time point and genotype. Whole-mount β-galactosidase staining. (**k–v**) Sections through E12.5 PPFs. (**x**) Section through E16.5 diaphragm. Asterisk in **b** shows location of Video S1. Arrow in **s** shows Gata4+ septum transversum. (**a–j, w**) Dorsal at top. Heart and lungs removed. (**k–v**) Dorsal at top, medial at left. Scale bar = 100 μm (**k–v**), 20 μm (insets **k–p**), 500 μm (**w**), 50 μm (**x**). CT, central tendon; E, esophagus; Lu, lung; NT, neural tube; PPFs, pleuroperitoneal folds; So, somite, ST, septum transversum.

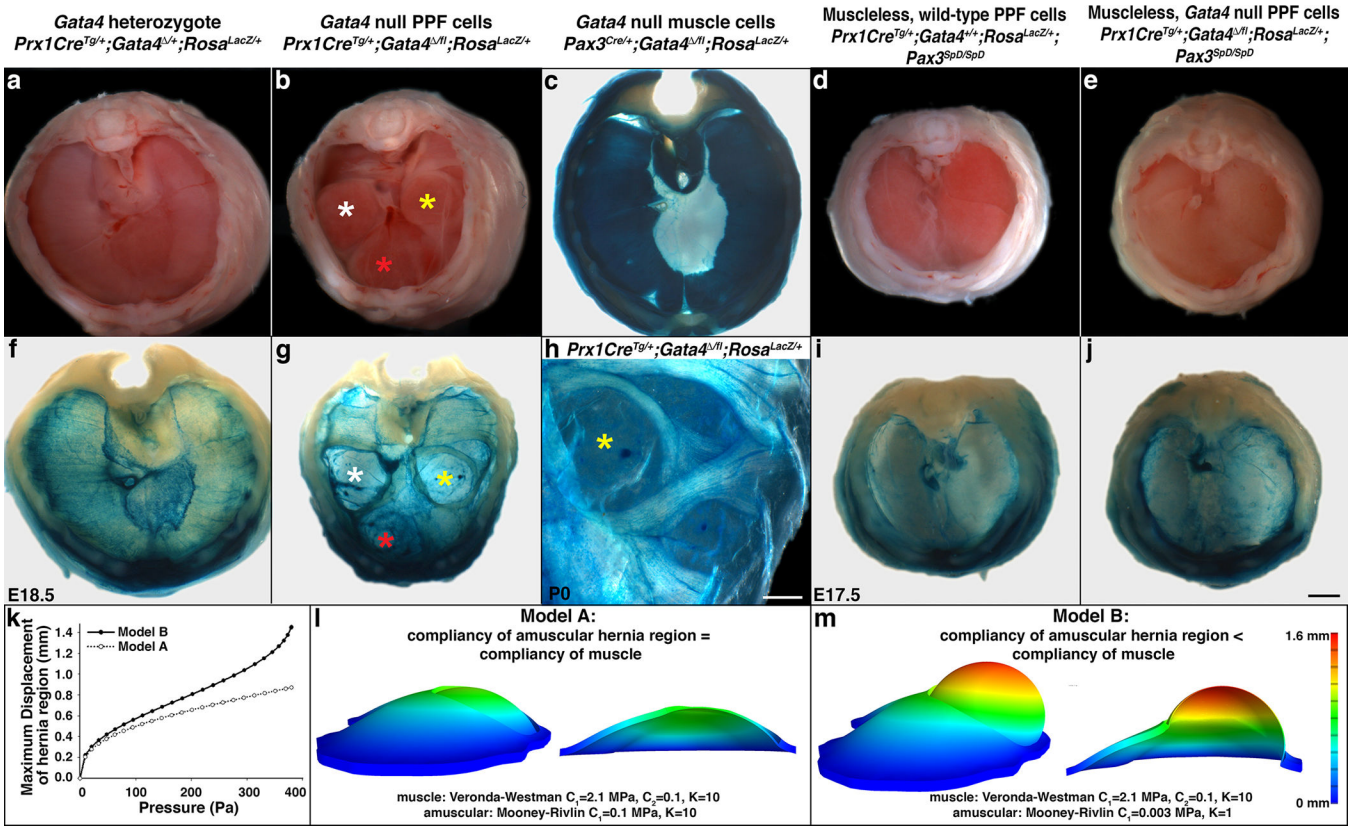

Fig. 2. Deletion of *Gata4* in the PPFs produces localized amuscular regions that are weaker than juxtaposed muscular regions and results in CDH

(**a–d**) CDH develops in mice with *Gata4* null PPF cells (n > 33/33; Bochdalek hernias labeled with white and yellow asterisks and Morgagni hernia labeled with red asterisk in **b**), but not in *Gata4* heterozygotes (n > 66/66; **a**), mice with *Gata4* null muscle (n = 28/28; **c**), or mice with muscleless diaphragms (n > 10/10; **d**). (**e, j**) Loss of muscle in diaphragms with *Gata4* null PPF cells rescues herniation, indicating that juxtaposition of amuscular with muscular regions is required for CDH (n = 3/3). (**g–h**) In herniated regions PPF cells are present, but muscle is not (n = 7/7). (**k–m**), Finite element modeling shows that a hernia only develops when the amuscular region is more compliant than the muscular region. Models are lateral views (**c, f–j**) Whole-mount β-galactosidase staining. (**a–j**) Dorsal is at top. Scale bar = 1 mm (**a–g, i–j**), 0.5 mm (**h**).

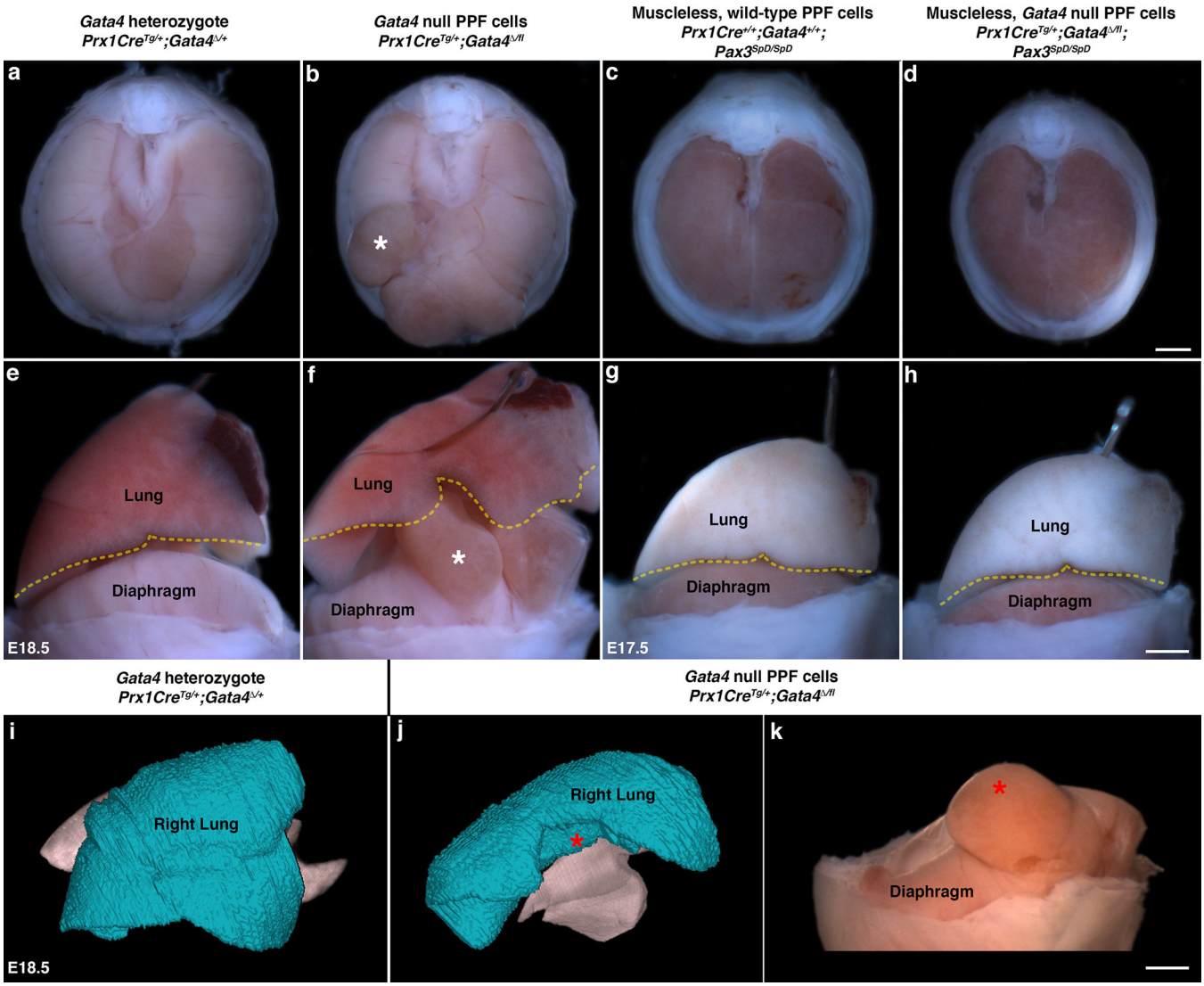

Fig. 3. In CDH, physical impedance by herniated tissue causes lung hypoplasia

(**a–b, e–f**) As compared with lungs in mice with a normal diaphragm (n > 50; **a, e**), development of lung lobar structure is impeded by liver herniated through a defective diaphragm (n = 8/8; white asterisks show equivalent herniated region in **b, f**). (**c–d, g–h**) Lungs develop normally in mice with a muscleless diaphragm (n > 5/5; **c, g**) or with a muscleless diaphragm with Gata4 null PPF cells (n = 2/2; **d, h**). (**i–k**) MicroCT scans show that lungs (**i–j**) are greatly reduced in presence of hernia (red asterisks show herniated region **j–k**; n = 3). (**i–j**) Lateral right view of lungs, right lungs shown in blue. (**k**) Lateral view of diaphragmatic hernia associated with malformed lungs (**j**). (**a–b, e–f, i–k**) E18.5. (**c–d, g–h**) E17.5. Scale bar = 1 mm (**a–d**), 1 mm (**e–h, k**).

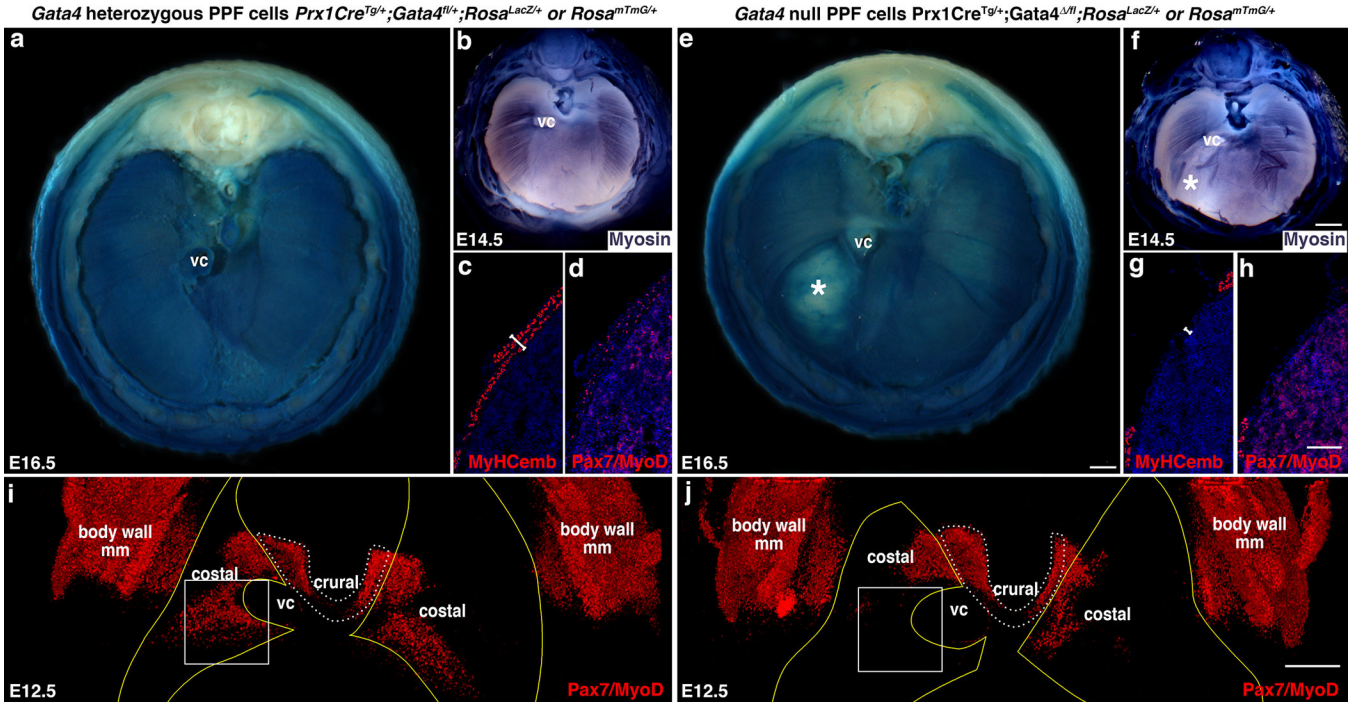

Fig. 4. CDH results from early defects in the localization of muscle progenitors

(**a, e**) Overt liver herniation through diaphragms with *Gata4* null PPF cells first appears at E16.5 (* in **e**, n = 3/3). (**b–d, f–h**) At E14.5 differentiating myofibers are aberrant (* in **f**; n = 7/7; **b, f**) and myofibers (**c, g**) and Pax7+/MyoD+ muscle progenitors (**d, h**) are absent in localized regions (n = 1/1). (**i–j**) At E12.5 Pax7+/MyoD+ muscle progenitors are absent in localized regions, particularly in the region (box) that consistently gives rise to hernias (n = 7/7). Pleuroperitoneal folds are outlined in yellow (outline derived from GFP immunofluorescence shown in Fig. 6a and b) and costal muscle is outlined in white dashed lines. (**a, b**) Whole-mount β-galactosidase staining. (**b, f**) Whole-mount myosin-alkaline phosphatase staining. (**c–d, g-–h**) Section immunofluorescence. (**i-j**) Whole-mount immunofluorescence (same diaphragms shown in Fig. 6a and b). (**a–b, e–f, i–j**) Dorsal is at the top. Scale bar = 500 μm (**a, e**), 500 μm (**b, f**), 100 μm (**c–d, g–h**), 200 μm (**i–j**). VC, vena cava; body wall mm, body wall muscles.

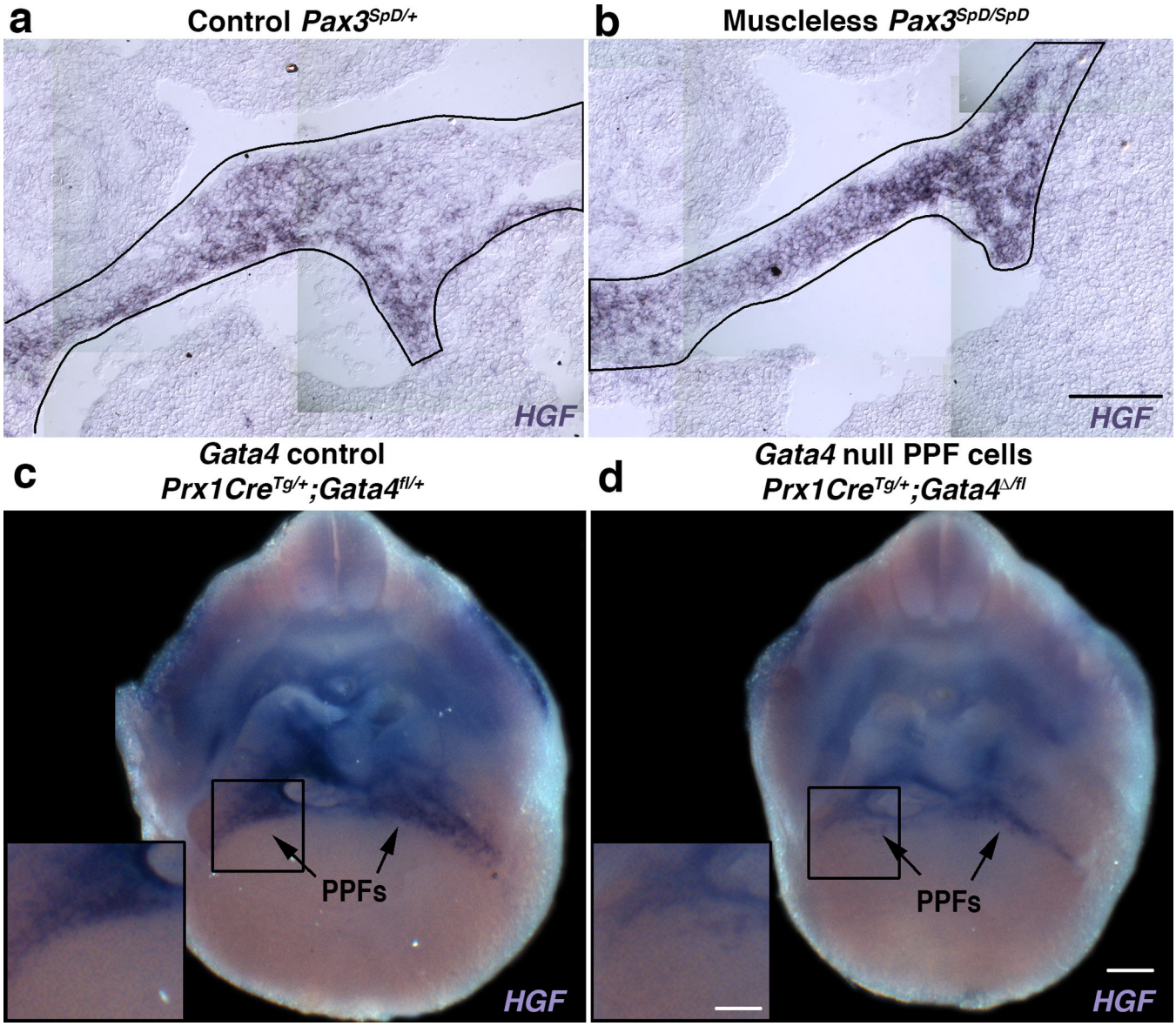

Fig. 5. HGF is strongly expressed in PPF cells and down-regulated in *Gata4* null fibroblasts

(**a–c**) *HGF* is expressed in PPF cells independent of muscle. PPFs are outlined in black. (**d**) Deletion of *Gata4* in PPF cells leads to *HGF* down-regulation, particularly in the region (box) that consistently give rise to hernias. (n = 11/11). Dorsal is at top of all panels. Scale bar = 100 μm (**a, b**), 250 μm (**c, d**) and 125 μm (insets **c, d**).

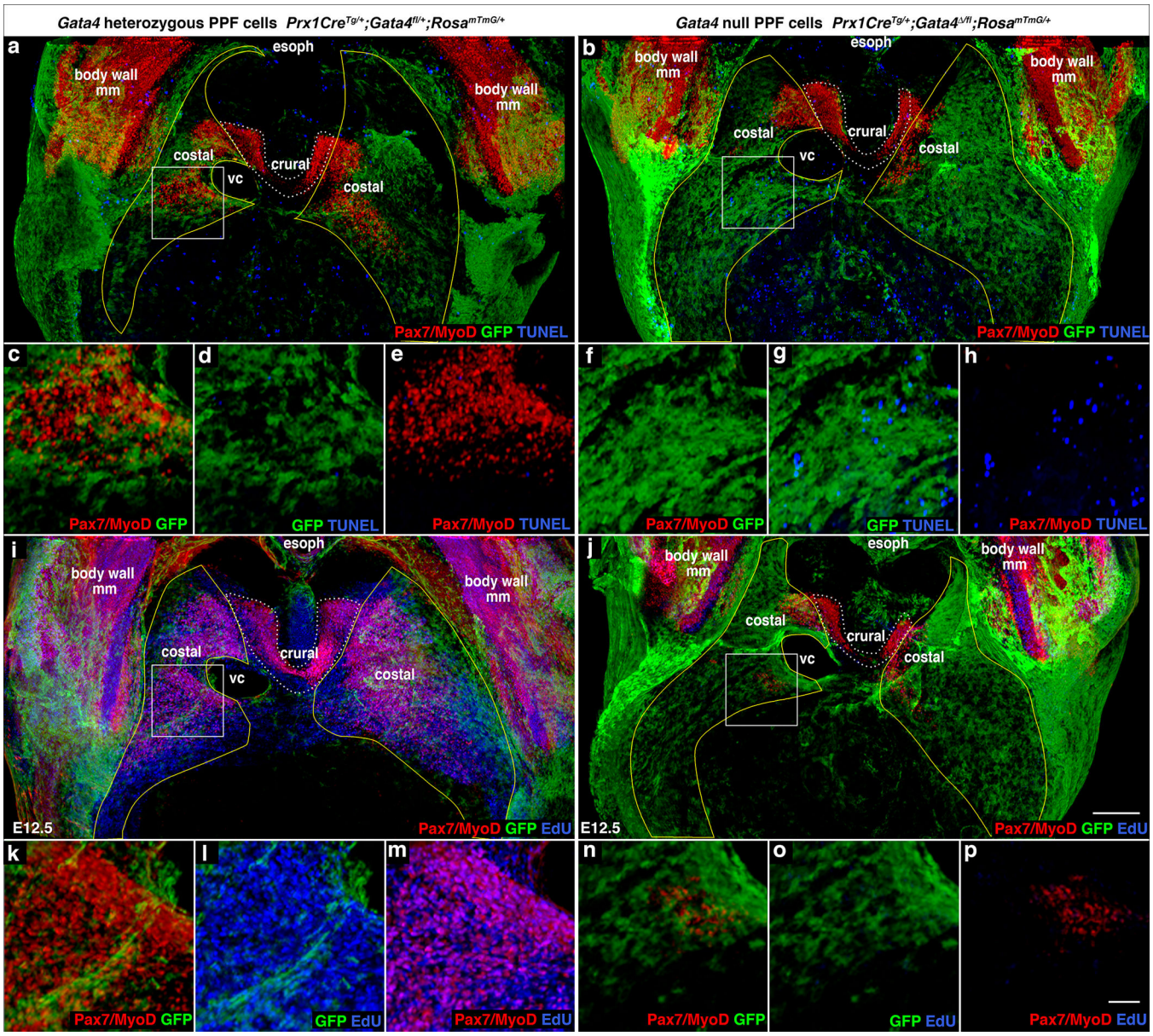

Fig. 6. Early defects in proliferation, apoptosis, and localization of muscle progenitors lead to CDH

(**a–h**) At E12.5 there is a marked increase in apoptotic cells in diaphragms with *Gata4* null PPF cells (**b, f–h** versus **a, c–e**), particularly in the region (boxes **a** and **b**, magnified **c–e, f–h**) that consistently gives rise to hernias (n = 3/3). (**i–p**) There also is a marked decrease in EdU+ proliferating cells in mutant diaphragms (n = 7/7). (**j, n–p** versus **i, k–m**). In the region (boxes **i** and **j**, magnified in **k–m, n–p**) destined to give rise to hernias the few myogenic cells are EdU−. (**a–p**) Costal muscle progenitors are surrounded by GFP+ PPF cells in control diaphragms but are excluded from regions with GFP+ *Gata4* null PPF cells in mutant diaphragms, particularly in destined hernia regions (boxes **b, j** magnified **f–h, n–p**). (**a–p**) Whole-mount immunofluorescence. (**a–b, i–j**) Pleuroperitoneal folds are outlined in yellow and costal muscle is outlined in white dashed lines. (**a–p**) Dorsal is at top. Scale

bar = 200 μm (**a–b, i–j**), 50 μm (**c–h, k–p**). PPF, pleuroperitoneal fold; NT, neural tube; E or esoph, esophagus; So, somite; ST, septum transversum, VC, vena cava, body wall mm, body wall muscles.

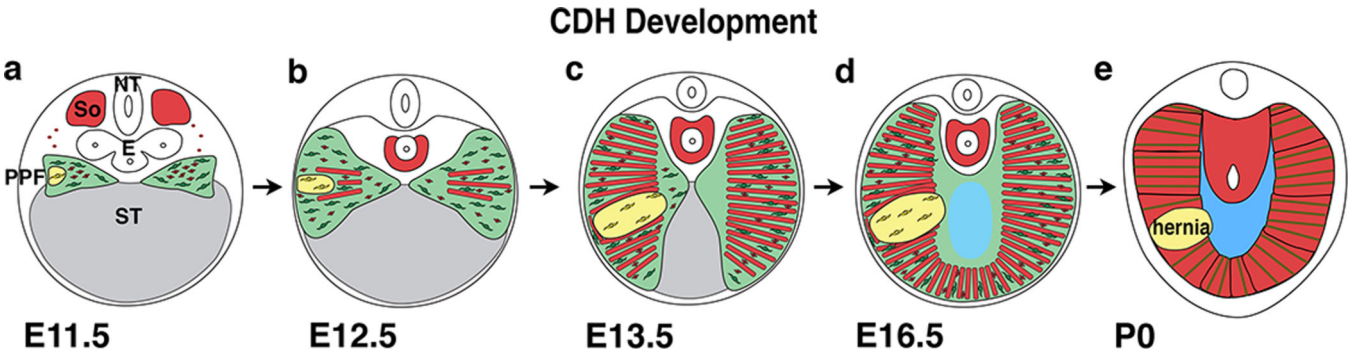

Fig. 7. Model of CDH development

Our data supports a model whereby CDH arises from early genetic mutations in a subset of PPF-derived muscle connective tissue fibroblasts (**a**; mutant fibroblasts are yellow, wild-type fibroblasts are green). Mutant fibroblasts clonally expand and inhibit muscle progenitors from developing in these regions (via decreased proliferation and increased apoptosis of muscle progenitors) and results in local regions (shown in yellow) that are amuscular, but contain connective tissue fibroblasts and their associated extracellular matrix (**b–d**). Amuscular regions are thinner and more compliant than surrounding thicker and stiffer muscularized diaphragm and allow herniation of abdominal contents into the thoracic cavity (**d–e**).